GEOMATICS, NATURAL HAZARDS AND RISK, 2018
VOL. 9, NO. 1, 16–32
https://doi.org/10.1080/19475705.2017.1405849

Taylor & Francis
Taylor & Francis Group

Lightning risk assessment at high spatial resolution at the residential sub-district scale: a case study in the Beijing metropolitan area

HaiBo Hu[a], JingXiao Li[b] and Xiya Zhang[a]

[a]Institute of Urban Meteorology, China Meteorological Administration (CMA), Beijing, China; [b]Beijing Lightning Devices Security Test Center, Beijing Meteorological Bureau, Beijing, China

ABSTRACT

Lightning risk indexes identifying the potential number of dangerous lightning events (NDLE) and ground sensitivity to lightning in residential sub-districts in the Beijing metropolitan area have been estimated on a 5 m resolution grid for the first time. The gridded cloud-to-ground (CG) lightning strike density was used in the NDLE calculation, on account of the multiple contacts formed by CG events with multiple lightning flashes. Meanwhile, in the NDLE estimates, the critical CG strike densities derived from the lightning location system data were corrected for network detection efficiency (DE). The case study for a residential sub-district indicates that the site-specific sensitivity to lightning, which is determined by the terrain factors related to lightning attachment and the lightning rod effects induced by nearby structures, differs greatly among types of underlying ground areas. The discrepancy in the NDLE, which is the numerical product of sensitivity and CG strike density, is dominated by the sensitivity to the relatively stationary CG strike density at the residential sub-district scale. Conclusively, the visualization of lightning risk sensitivity and NDLE differences in parts of a residential sub-district at a high spatial resolution makes this model useful in risk reduction and risk control for lightning risk management.

ARTICLE HISTORY
Received 27 April 2017
Accepted 31 October 2017

KEYWORDS
Lightning risk; CG flash density; lightning detection efficiency

1. Introduction

The frequent occurrences of lightning disaster events cause large numbers of casualties and substantial damage losses, such that lightning is considered one of the most dangerous natural hazards (Curran et al. 2000; Holle et al. 2005; Zhang et al. 2011) and the second most fatal meteorological phenomenon (Ashley and Gilson 2009). Lightning risk assessment is meant to investigate and locate high-risk areas, enabling the implementation of mitigation measures for lightning risk reduction (Kaplan and Garrick 1981; Hu et al. 2014). Previously, we developed a lightning risk zoning model based on 1 km resolution grids (Hu et al. 2014). The lightning risk recognition at that scale, however, does not appear to be fine enough to reflect the lightning risk characteristics that are useful in disaster preparedness, especially in densely populated urban areas. Thus, it is desirable to assess lightning risk at an extremely high resolution (e.g. a 5 m spacing grid) at the residential sub-district scale in order to identify risk discrepancies in detail, which have significance for risk control and risk reduction (Mills et al 2010).

High spatial resolution enables deliberately locating specific underlying areas, especially in densely populated urban areas. Thus, high resolutions improve the estimates of ground sensitivity

CONTACT HaiBo Hu hbhu@ium.cn

to lightning, which is correlated with certain environmental settings, such as topographical features and distribution of earthen structures (Rizk 1994; Vogt 2011). Approaches will be employed in pattern recognition of topographical features, locating earthen structures and determining their lightning collection areas, downscaling grids of cloud-to-ground (CG) strike densities, among others. These processes can be accomplished with the support of GIS technology using high-resolution map data. Natural lightning CG strikes are obvious drivers of lightning-related disasters. Lightning climatology, which preliminarily denotes lightning risk, should be quantified for risk assessment (Bogdan and Burcea 2010). The approach is to derive lightning parameters (e.g. CG flash/strike density and CG flash multiplicity) from observational data, e.g. climatological data (Changnon 1985; Gabriel and Changnon 1989), remote sensing lightning imagery (Christian et al. 2003) and lightning location system (LLS) data (Changnon 1993; Schulz et al. 2005; Biagi et al. 2007; Cummins and Murphy 2009). These lightning parameters fundamentally reflect regional lightning activity relevant to lightning disaster occurrence (Schulz et al. 2005; Mäkelä et al. 2010). They are critical in confirming lightning risk even at the residential sub-districts scale.

As a premise of risk recognition, lightning characteristics should be revealed mostly by introducing LLS data, on account of its high spatial-temporal resolution (e.g. Krider et al. 1980). Then, the lightning risk characteristics can be obtained by overlapping the lightning characteristics (CG flash/strike density) with other risk factors (e.g. sensitivity and exposure) (Hu 2014).

Lightning risk is linked to the combined effects of regional lightning activities and ground sensitivity to lightning. Risk recognition at high resolution can provide visualizations for the decision-making in risk management. It facilitates risk-reduction strategies that are practicable in disaster prevention (Smith 1996). For a residential sub-district, the visual lightning risk recognition can provide information in a form that is straightforwardly understandable to local decision and policy-makers. Moreover, this site-specific lightning risk is critical to public safety and infrastructure planning (Stallins and Rose 2008).

2. Data description

2.1. Lightning location system (LLS) data

LLS data collected from 2007-2016 by the ADTD (Advanced TOA and Direction system; TOA denotes time-of-arrival) deployed by the China Meteorology Administration (CMA) were used to derive the CG flash/strike density. These data include time, location, peak current and polarity of CG lightning strikes.

The ADTD consists of more than 301 sensors (as of March 2011) in China (Yao et al. 2012). In Beijing, 9-14 ADTD-1 sensors [improved IMPACT [combined MDF (magnetic direction finding) and TOA] sensors] can detect 1–450 kHz (the very low-frequency band) lightning sources (Figure 1). The ADTD-1 sensors use the combined MDF and TOA method for position retrieval. In this method, if a lightning source is only detected by two ADTD-1 sensors, the algorithm uses one TOA hyperbolic curve and two MDF vectors to retrieve the position. If it is detected by three sensors in a non-duplicate region, the TOA algorithm is used to retrieve the position directly, whereas the TOA is first used to find a duplicate location, then the MDF is used to find the true location. If a lightning event is detected by four or more sensors, a TOA least square method is used to retrieve a more precise position. Thus, the location precision of the lightning source reported by four or more sensors is better than that reported by fewer sensors. In our LLS data, the percentage of lightning sources reported by four or more sensors relative to the total number of detected sources is 66.815%. Meanwhile, the ADTD-observed +CG and –CG lightning peak currents are in the ranges of 0.08–995.9 and 0.258–992.6 kA, respectively (Figure 1).

The manufacturers claimed that the detection efficiency (DE) of ADTD sensors could be 90% at distances between 300 and 600 km, with a median location accuracy error of 1 km. However, only the flash DE can be 90%, whereas the strike detection efficiency (SDE) is lower. The first strike peak current in a multiple-strike CG flash can be greater than twice its subsequent strike peak current

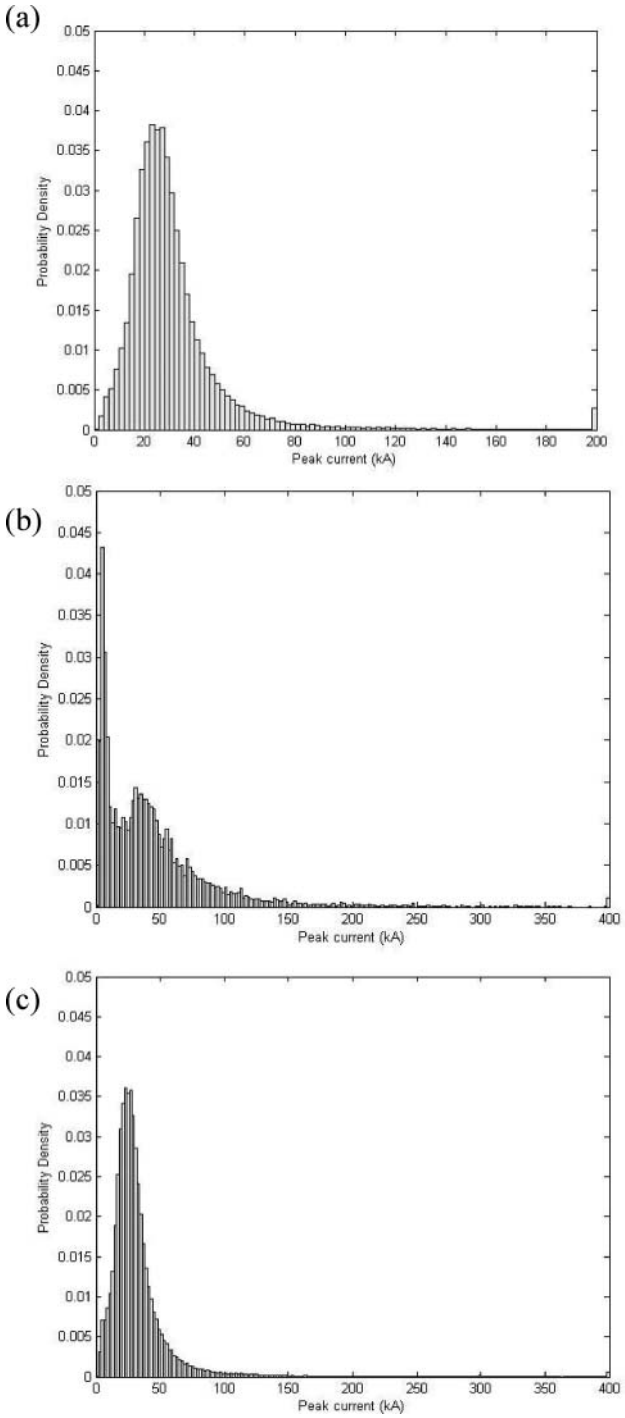

Figure 1. Histogram of peak current probability density of (a) –CG lightning, (b) +CG lightning and identified +IC lightning on account of their peak currents less than 15 kA, and (c) total CG lightning.

(Rakov and Uman 1990). Thus, the sensors can capture the first larger peak strike but missing the weaker subsequent strike (Rudlosky and Fuelberg 2010). Moreover, some weak CG strikes (including single-strike CG flashes) cannot be detected due to signal attenuation induced by long-distance propagation and terrain factors (Schütte et al. 1988), among other factors.

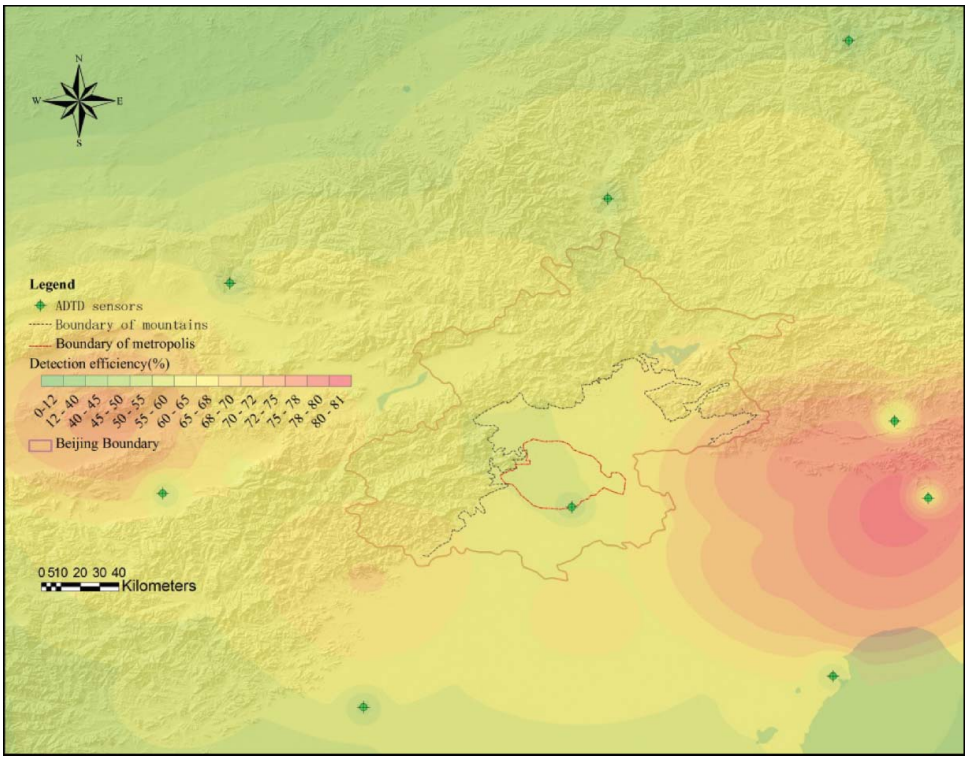

Figure 2. Distribution of the DE estimates and sensors of the ADTD around the Beijing district (enclosed by scarlet lines). The SDEs in the Beijing metropolitan area (red lines) are almost all above 55% and are lower than those in the surrounding areas, whereas the peak SDE zones located to the east of the metropolitan areas possess a maximum SDE of 81.1%. (This figure is available in colour online.)

Because the strike number is critical in lightning risk estimates (Bertram and Mayr 2004), we estimated the SDEs of the ADTD in grids (1 km × 1 km, see Figure 2) and corrected the lightning strike density using the SDE. The SDE estimates approximate those of the U.S. National Lightning Detection Network (NLDN) in 1998, which was reported to be 62% (Idone et al. 1998). Hence, the DE level of the ADTD is equivalent to that of the NLDN, at least in 1998, indicating that considerable improvement remains in terms of network upgrades.

2.2. Other data

Digital elevation model (DEM) data were used to identify site-specific lightning attachment capabilities related to topography (Vogt 2011). The 30 m spatial resolution basically meets the requirements for identifying hypsographic features and confirming terrain factors.

Additionally, basic GIS maps with scales of 1:2,000 in urban settings and 1:50,000 in rural settings have been used to measure the lightning collection areas of structures based on the geometric shape and height of the structure, which are readily available in GIS map layers (Hu et al. 2014). The GIS map-layer data-set has a structure-type field that can be used to determine the lightning protection capability of structures.

3. Methods

The lightning risk index of the potential number of dangerous lightning events (NDLE) can be reserved for lightning risk zoning at the residential sub-district scale. Correlated to regional

lightning activity and site-specific sensitivity to lightning, the NDLE, i.e. N_x, can generally be estimated as (Hu et al. 2014)

$$N_x = K \times N_g \times A_d, \tag{1}$$

where K denotes the coefficient related to the environmental setting; N_g denotes the CG lightning strike density (strikes/yr·km^2); and A_d denotes the collection area of the lightning strike, mostly determined by site-specific lightning attractiveness variably based on the type of underlying ground area. Because each strike in a multiple-strike CG flash can produce damage losses and/or casualties, it is reasonable to treat N_g as the CG strike density (strikes/yr·km^2).

3.1. CG lightning strike density corrected for DEs and downscaling

3.1.1. Network DE estimation

The network DE is determined by the performance and sensitivity of the sensors, the sensor network geometry, and the underlying ground conductivity (Schütte et al. 1988; Naccarato and Pinto 2009; Mäkelä et al. 2010), among other factors. The use of DE estimates to correct CG flashes/strikes and evaluate the LLS network performance involved a series of methodologies published in the literature (e.g. Cummins et al. 1998; Schütte et al. 1988; Naccarato and Pinto 2009). Although DE can be determined more precisely with observations based on live information on lightning occurrences (e.g. video or tower measurements), this approach has only been experimentally utilized to produce localized DE estimates (Saraiva et al. 2010; Visacro et al. 2010; Warner et al. 2013). The methods of DE estimates using theoretical models are more convenient and applicable in comprehensively confirming a network DE. Schütte et al. (1987, 1988) introduced the Weibull distribution for estimating the signal strength acceptance levels for sensors, and this method can be used for network DE calculations. Cummins et al. (1998) also combined the peak current cumulative distribution with a signal-propagating model to estimate the absolute flash DE for the NLDN. Naccarato and Pinto (2009) deduced the DEs using the individual DE probability distribution functions of the sensors based on samples of CG strike data detected by a large network while considering different distances from the sensors and specific peak current ranges.

We calculated the DEs of the ADTD in grids accounting for the network performance and sensitivity based on the distances and azimuths among the sensors. The CG lightning peak currents were converted to signal strength with arbitrary units (a. u.) using the method of Schütte et al. (1988), which linearly measures the signal strength with signal propagating distance. Schütte et al. (1987) confirmed the Weibull distribution of lightning signal strength.

Thus, methodologically, the signal acceptance of a sensor can be given by

$$A(r) = \begin{cases} 0 & r < cr_0/s_{\max} \\ 1 - \exp\left[-\left(\dfrac{s_{\max} r/r_0 - c}{a}\right)^b\right] & cr_0/s_{\max} < r \le cr_0/s_{\min} \\ \exp\left[-\left(\dfrac{s_{\min} r/r_0 - c}{a}\right)^b\right] - \exp\left[-\left(\dfrac{s_{\max} r/r_0 - c}{a}\right)^b\right] & r > cr_0/s_{\min} \end{cases}, \tag{2}$$

where $s_{\min}$ and $s_{\max}$ are the lower and upper signal threshold, which will be 20 and 600 a. u., respectively; r_0 is the standard distance, which will be 100 km; r is the distance to the sensor; and a, b, and c are the scale, the shape and the location parameter of the Weibull distribution of signal strength, respectively (Schütte et al. 1987, 1988).

Only two ADTD IMPACT sensors reporting a strike are required to obtain a valid solution. Thus, the DE on a grid cell can be determined as (Naccarato and Pinto 2009)

$$A = A_1(r_1) \times A_2(r_2) \quad A_1 \text{ranked} \quad A_1(r_1) \ge A_2(r_2) \ge A_3(r_3) \ge \ldots \tag{3}$$

where $A_i(r_i)$ denotes the acceptance of one sensor; r_i (i = 1, 2, 3, ...) is the distance of the ith nearest sensor to the grid cell center and A the grid cell DE of the network.

3.1.2. CG strike density correction

The CG strike density N'_g directly derived from LLS data can be corrected for the DE of the ADTD using the following equation:

$$N_g = \frac{N'_g}{D_g}, \tag{4}$$

where N_g is the corrected CG strike density and D_g is the DE of the grid.

The CG strike density in the high-resolution (e.g. 5 m) grid could be downscaled from a coarse (e.g. 1 km) grid or derived directly from the LLS data using a kernel density estimator. Usually, when the location error of each CG lightning strike observed by LLS is given, the probabilistic computational methods based on confidence ellipse are recommendable for deriving CG strike densities in high spatial resolution (Bourscheidt et al. 2014; Etherington and Perry 2017). However, the ADTD doesn't provide the location error of single CG lightning strike. We are obliged to use a bivariate (XY) kernel density method to estimate the CG lightning strike density at the 5 m resolution, which the kernel is assumed to be Gaussian. The ArcGIS software provides the tool of kernel density estimator (Refer to http://desktop.arcgis.com/en/arcmap/10.3/tools/spatial-analyst-toolbox/kernel-density.htm). In the parameterization of kernel density function, the cell-size is set to 5 m, and the search radius is 1000 m, which corresponds to the magnitude of the ADTD median location accuracy error.

Supplementarily, the approach of inverse distance weighting (IDW) are also used to interpolate the CG strike density from the larger grid (with 1 km spacing), in which 9 grid cells were involved, i.e. the center, up, down, upper left, upper right, left, right, lower left, and lower right 1 km × 1 km grid cells. Mathematically, the interpolation can be described as

$$N_{g5m} = \sum_{i=1}^{n} N_g(i).\frac{1/r(i)}{\sum_{i=1}^{n} 1/r(i)}, \tag{5}$$

where N_{g5m} is the interpolated CG strike density in a 5 m spaced grid cell; n ($n \leq 9$) is the number of strike-containing cells and the approximately 1 km spaced grid cells; $N_g(i)$ is the CG strike density of the ith 1 km spaced grid cell; and $r(i)$ is the distance of the central point of the 5 m grid cell to that of the ith 1 km spaced grid cell.

3.2. NDLE estimates for the 5 m spacing grids

We calculated the NDLE for an earthen structure, an outdoor area under a structure canopy (OAUSC) and an open-field area (OFA). Because these types of underlying ground areas differ in lightning protection capability, lightning attractiveness, and lightning attachment induced by top terrains, different methodologies were used to estimate the NDLE. Additionally, the approaches were adjusted based on the conditions of the grids intersecting with these underlying areas (Figure 3). The spatial relationship of the underlying areas to the grids means that one grid box often covers only one unique underlying area and seldom covers multiple types of areas (Figure 3). Thus, the NDLE of each grid cell can be calculated directly using a GIS overlapping operator. This approach is different from that used for the 1 × 1 km sized grids, which is to sum the total NDLE of all areas of the large grid (Hu et al. 2014).

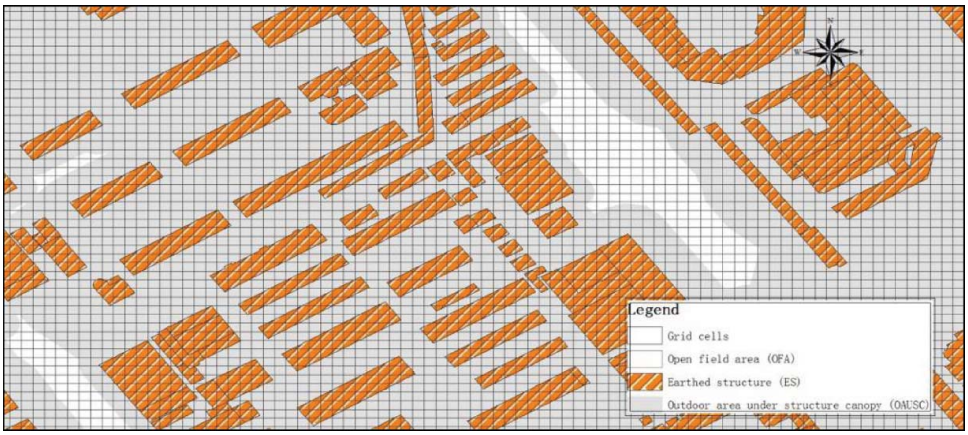

Figure 3. Samples of three types of underlying ground areas (i.e. earthen structure, OAUSC, and OFA) in a 5 m spaced grid displayed in GIS. (This figure is available in colour online.)

3.2.1. NDLE estimates of an earthen structure (ES)

The NDLE value of a structure N_d is calculated as follows (Hu et al. 2014):

$$N_d = N_g.A_d.C_d.P_d.10^{-6}, \tag{6}$$

where A_d (m^2) is the lightning collection area of a structure; C_d is the terrain factor, which is deduced using DEM data, accounting for its relationship to the surrounding topography (see Table 1); and P_d is the coefficient representing the lightning protection capability of the structure.

Given the structure height in metres H, the collection area A_d can be determined as follows (Rizk 1994):

$$A_d = 670.8\pi H^{0.96}. \tag{7}$$

The structure protection capability includes protecting 1) living beings from being injured by a lightning strike, 2) the structure from physical damage, and 3) the internal systems in the structure. Substantially, these capabilities are represented by the casualty probability p_a, the physical damage probability p_b, and the internal systems failure probability p_c in risk estimates. Herein, for simplification, the lightning risk assessment only takes into account p_a, i.e. $P_d = p_a$.

The casualty probability due to touch and step voltage induced by lightning striking the structure reflects the structure's Lightning Protection Level (LPL), which can be deduced by accounting for the lightning protection measures taken by the structure (Table 2).

We listed the protection measures that would be probably taken by 10 structure types in Beijing (see Table 2) available in a GIS map-layer data-set. Most structures are equipped with lightning rods. Some concrete steel structures have iron infrastructure and framework as the lead-in wire for

Table 1. Estimating the terrain factor of a structure based on its surrounding topography (defined by IEC62305-2 2010).

Description of the surrounding topography	C_d
Higher than the top of the structure	0.25
As high as the top of the structure	0.5
On flat ground	1
On top of a hill	2

Table 2. The structure types corresponding to the lightning protection capability in Beijing.

Structure type	GIS identity	Protection measures	p_a
General building	211	Iron infrastructure and framework as a lead-in wire structure.	10^{-4}
General structure with basement	21109	Same as above	10^{-4}
Bunk house	212	Effective soil equipotentialization	10^{-2}
Bunk house with basement	21209	Same as above	10^{-2}
Bridge gallery	218	Electrical insulation of exposed downward conductor	10^{-2}
Special house	229	Iron infrastructure and framework as a lead-in wire structure	10^{-4}
Special house with basement	22909	Same as above	10^{-4}
Ruined house	214	No protection measures	1
Hut	215	Same as above	1
Public lavatory	3551	Electrical insulation of exposed downward conductor	10^{-3}

lightning protection. Thus, they possess a better capability of protecting living beings from lightning strike injuries.

3.2.2. NDLE estimates of an outdoor area under a structure canopy (OAUSC)

Under these conditions, the NDLE value, i.e. N_{Dc}, can be calculated as follows:

$$N_{Dc} = N_g.A_{Dc}.C_d.C_c.10^{-6}, \tag{8}$$

where A_{Dc} (m^2) is the intersection area of the OAUSC and the grid cell; C_d is the terrain factor of the grid cell; and C_c is the coefficient representing lightning rod effects produced by the surrounding structures. At a fine grid scale (e.g. 5 m), its calculation is simplified as follows (Petrov and D' Alessandro 2002):

$$C_c = \frac{1}{\sum_{i=1}^{n} H(i)}, \tag{9}$$

where $H(1)$,..., $H(n)$ are the floor numbers of the surrounding structures, whose canopies cover the grid cell. It is reasonable that C_c will approximate zero if the grid cell is under canopies of many nearby tall structures.

3.2.3. NDLE estimates of an open-field area (OFA)

Because they are totally exposed to lightning strikes, OFAs are more susceptible to lightning. Thus, the NDLE, N_{Ds}, can be estimated as follows:

$$N_{Ds} = N_g.A_{Ds}.C_d.10^{-6}, \tag{10}$$

where A_{Ds} is the intersection area of the OFA and the grid cell.

3.2.4. NDLE estimates in a grid cell

After the NDLE values of the three types of underlying ground areas are calculated, the NDLE of a grid cell intersecting with these areas, *Nd_Cell,* can be calculated as follows:

$$\begin{aligned} Nd\_\text{Cell} = {} & N_d \times \text{Intersect}(\text{Area\_Cell}, \text{Area\_ES}) \\ & + N_{Dc} \times \text{Intersect}(\text{Area\_Cell}, \text{Area\_OAUSC}) \\ & + N_{Ds} \times \text{Intersect}(\text{Area\_Cell}, \text{Area\_OFA}) \end{aligned}, \tag{11}$$

where Area_Cell, Area_ES, Area_OAUSC, and Area_OFA denote the geometries of the grid cell, the earthen structure, the outdoor area under structure canopy, and the OFA in the grid cell, respectively. *Intersect* is a GIS operator for calculating the intersection areas of the grid cell and the geometries of the three types of underlying ground areas (i.e. the structure, the outdoor area under structure canopy, and the OFA), respectively.

3.3. Parameters reflecting lightning risk characteristics

The lightning risk assessment is to estimate the NDLE and sensitivity and to subsequently identify high-risk areas. Then, pertinent advice can be given to decision-makers who will undertake measures for lightning risk mitigation in residential sub-districts.

The CG strike density, N_g, ground sensitivity to lightning, S_x, and the NDLE, N_d, essentially reflect the lightning risk characteristics of a local community, which are critical for decision-making in lightning risk management. The CG strike density, N_g, an indicator of regional lightning activity, can be derived from the LLS data. The NDLE value, a numerical product of the CG strike density, N_g, and sensitivity, S_x, reflects the site-specific lightning hazards.

The sensitivity is defined as an indicator of the lightning strike susceptibility of the underlying ground and is mostly correlated to land-surface characteristics, e.g. terrain features and distribution of earthen structures. Based on site-specific environmental settings rather than regional lightning activity, the sensitivity can be calculated as follows:

$$S_{\mathrm{d}} = A_d \bullet C_d \bullet P \bullet 10^{-6}, \tag{12}$$

$$S_{\mathrm{Dc}} = A_{Dc} \bullet C_d \bullet 10^{-6}, \tag{13}$$

$$S_{Ds} = A_{Ds} \bullet C_d \bullet 10^{-6}, \tag{14}$$

where S_d, S_{Dc}, and S_{Ds} are the lightning sensitivity for a structure, an OAUSC and an OFA, respectively. Differences in the NDLE in a sub-district are mostly determined by the sensitivity, due to the relative constant values of CG strike density. In this context, the sensitivity and the NDLE jointly indicate the lightning risk at a high resolution.

4. Analysis on lightning characteristics

Lightning climatology preliminarily reflects lightning risk characteristics but does not account for sensitivity and exposure to lightning (Ashley and Gilson 2009). Analysis of lightning characteristics is the premise of risk assessment even at the sub-district scale, as it can provide critical parameters for lightning risk assessment, e.g. the CG flash/strike density and CG multiplicity. We derived the lightning parameters from the ADTD data by counting the annual CG flash/strike numbers in 1 km grids. The CG strikes were grouped into flashes based on a multiplicity delay of 1 s within a radius of 20 km (Cummins et al. 2006; Drüe et al. 2007), and +CG flashes with a peak current of less than 15 kA were classified as IC lightning (recommended by Cummins and Murphy 2009).

Convection events are usually enhanced by orographic uplift in the mountains, which trigger more CG strikes (Bourscheidt et al. 2009). However, the derivation from the ADTD data exhibits relatively lower CG flash/strike densities in the northern and western mountainous areas than in the plains, except for a relatively high density in the south-western mountains (Figure 4). The thunderstorms in urban areas on the plains can be enhanced by urban characteristics (e.g. roughness, aerosols, and urban heat islands) and consequently produce more CG flashes (Shepherd et al. 2002; Rose et al. 2008; Stallins and Rose 2008; Hu et al 2014; Hu 2015; Kar and Liou 2014), especially in the downwind areas (see the blue-circled in Figure 4(c)). Additionally, a high CG strike density distributed in upwind southern areas (see the purple-circled in Figure 4(c)) is observed. We assumed that

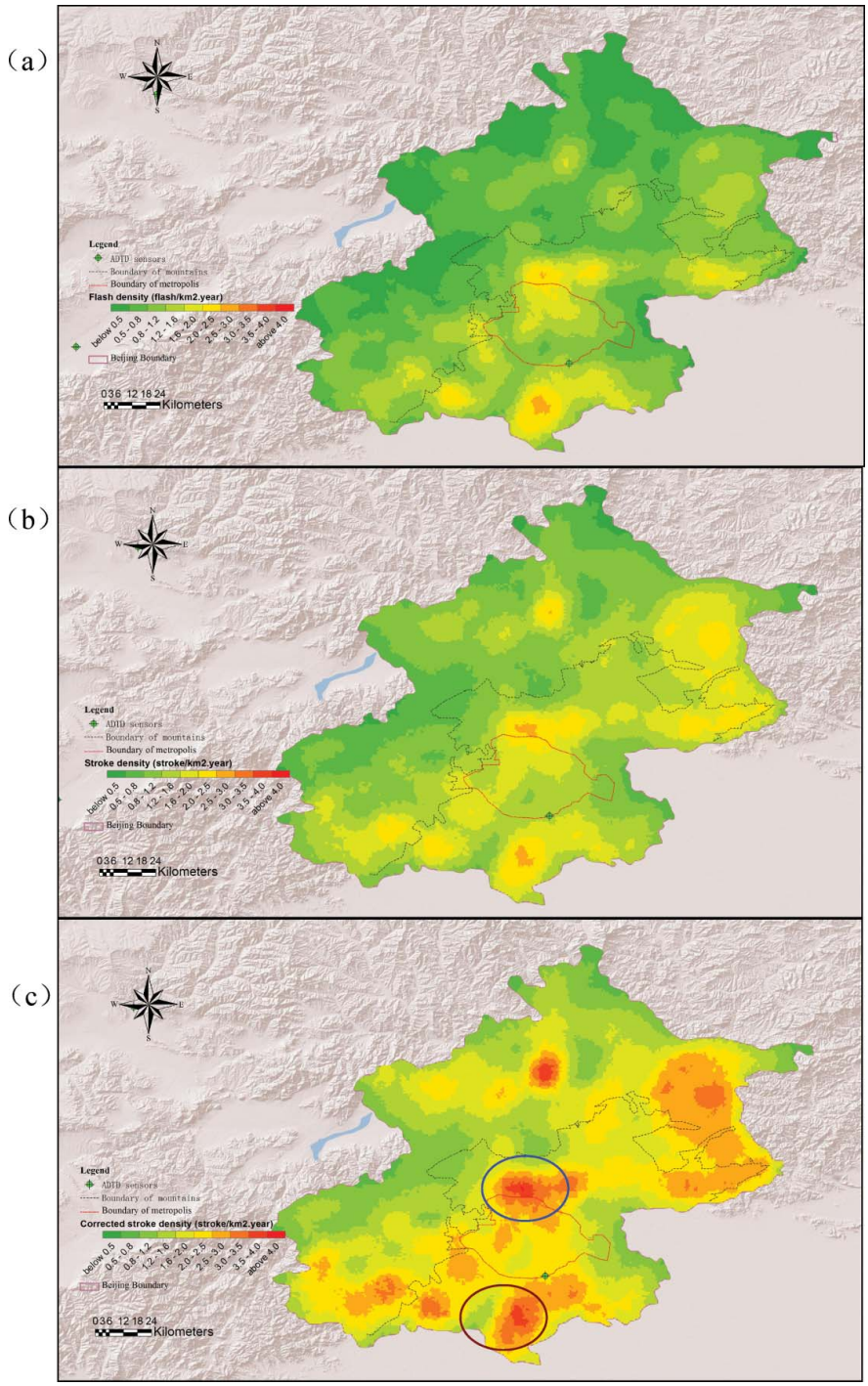

Figure 4. Distribution of (a) CG flash density (flash/yr·km^2), (b) CG strike density (strikes/yr·km^2), and (c) corrected CG strike density (strikes/yr·km^2). For convenience, the same legends for contours and shading were used in the CG flash density, CG strike density and corrected CG strike density plots. (This figure is available in colour online.)

this is related to random cloud condensation nuclei concentrations affecting cloud properties and the initiation of precipitation over cities (Steiger et al. 2002; Stallins et al. 2006; Kar and Liou 2014).

No matter what can explains the higher CG flash/strike density in the plains, the DE of an LLS cannot be 100% (Schulz et al. 2005; Mazarakis et al. 2008). The actual CG strike numbers in the grids, however, are critical to the NDLE estimation. Thus, we corrected the gridded CG strike densities for DEs to fit the actual values.

After being corrected using the deduced DEs (see Figure 2), the CG strike densities in the north-eastern mountains, metropolitan areas, southern plains and south-western mountains increased significantly in comparison with the uncorrected values (see Figure 4(b) and 4(c)). The corrected densities in metropolitan areas are mainly between 2 and 4 strikes/yr·km^2, which are higher than expected. However, a relatively high CG strike density remains in the plains.

Based on samples of LLS data, the probability distribution of lightning signal strength is critical to deducing the network DE. The LLS data observed in a limited period of time cannot provide a perfect probability distribution, which obviously can lead to biases in DE estimates. Moreover, the underlying surface conductivity is lower in mountains, and the lightning signal strength will be more attenuated in mountains than in plains. However, this attenuation cannot be precisely taken into account in DE estimates and, thus, leads to uncertainty. No matter how the DE estimates are effectively used for correcting CG lightning density derived from LLS data, it is still advisable that the network should be upgraded to improve the ADTD DEs and the detection accuracy. The anomaly of higher lightning density in the plains may be explained with additional evidence.

5. Case study of lightning risk assessment in a residential sub-district

The model running at a 5 m resolution can optimally cover a small area of 10-100 km^2. We selected two residential sub-districts in Beijing metropolitan areas for risk analysis, accounting for indicators of sensitivity and the NDLE. One is the sub-district of Malianwa in the north-western metropolitan areas and the foothills of the western YanShan Range. Its complex topography involves a diversity of ground sensitivities to lightning. The other is the Beijing International Airport, where the lightning risk discrepancy between the open fields of the aircraft parking areas and the terminal structure is remarkable.

5.1. Ground sensitivity to lightning

In terms of risk management, sensitivity recognition contributes to lightning risk avoidance on thunderstorm days. Additionally, it can be used to direct deployment of lightning protection facilities and systems (Schulz et al. 2005).

The lightning sensitivity zoning in the sub-district of Malianwa indicates that the sensitivity magnitudes of structures and outdoor areas under structure canopies are usually less than 0.15 (Figure 5(a)). Alternatively, if the terrain factors are not included, the greatest sensitivity is 1.0 on an open field in the plains (Figure 5(a)). Accounting for the terrain factors, the sensitivity in mountainous areas will increase to 1.15-1.3, for example, in the high sensitivity zones of western uplands of this sub-district (see *A* in Figure 5(b) and 5(c)). This higher sensitivity in the hills means that the CG strikes are more likely to occur at topographic highpoints by as much as 15%–30.0% when compared with random points in the plains. This increased sensitivity of topographic highpoints is somewhat in agreement with the findings of Vogt (2011).

As displayed in Google Earth, the sensitivity zones exhibit a good correlation with topographical features and the distribution of earthen structures (see Figure 5(c)). Especially, on account of the protection from the structures, the structure occupying areas as well as these under the structure canopies exhibit an abrupt lower sensitivity to lighting. A sensitivity buffer can be recognized between the earthed structure and its surrounding open field, where it forms a ring pattern of higher sensitivity values around these structures (see Figures 5 and 6(a)). Apparently, the simulated

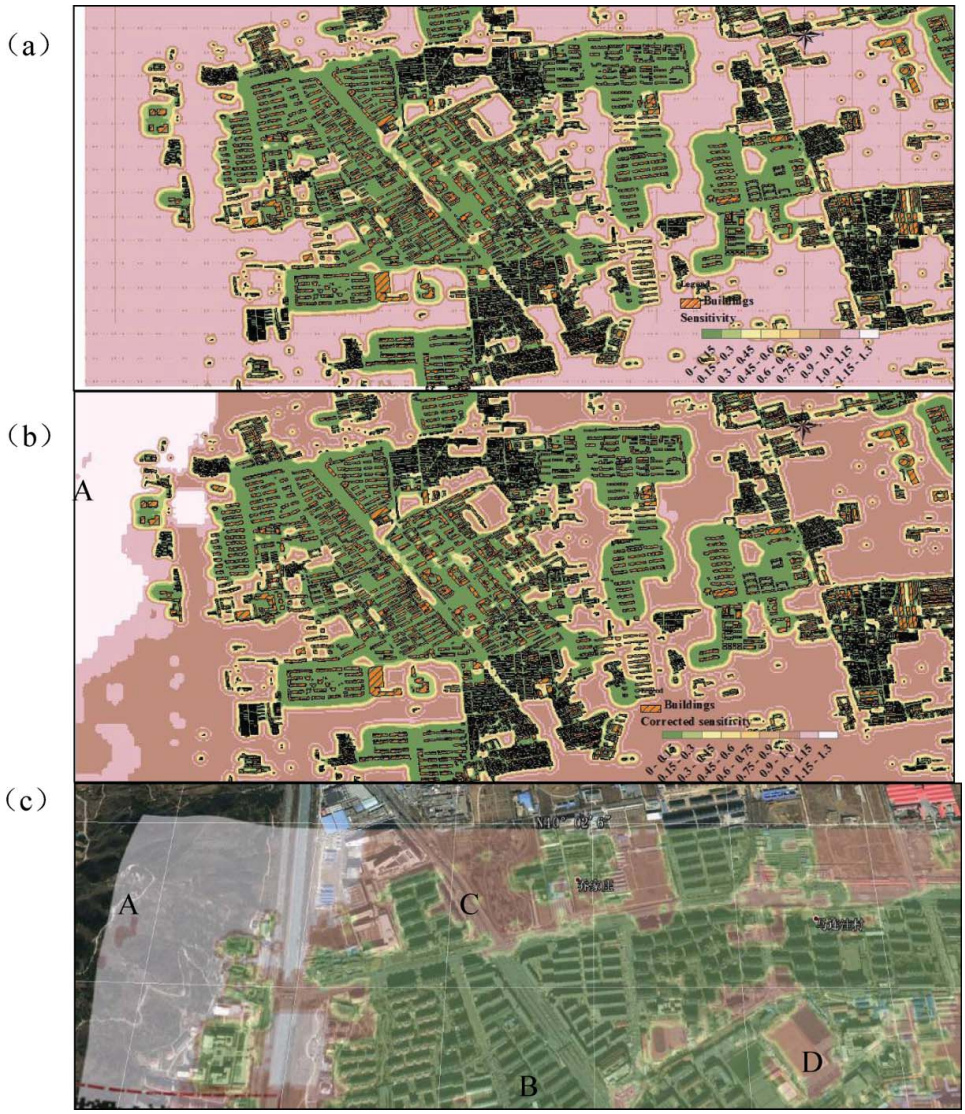

Figure 5. Sensitivity zones in the sub-district of Malianwa, in cases of (a) not accounting for the terrain factor, (b) accounting for terrain factors, and (c) displayed in Google Earth. These zones correspond well with the distribution of underlying structures and topographical features. For example, point *A* in the mountainous areas exhibits a high sensitivity, *B* in the dense structure area exhibits a lower sensitivity on account of the lightning rod effects produced by nearby structures, and *C* in an OFA exhibits a relatively high sensitivity. Interestingly, the sensitivity of point *D* at an open sports field is obviously higher than that of the surrounding densely built-up areas. (This figure is available in colour online.)

sensitivity is explicably in accordance with the settings, and it is valuable in visualizing lightning risk management.

5.2. NDLE

Similar to sensitivity, the NDLE values for a structure and an OAUSC are lower. The NDLE values for an OFA are equal or even magnitudes greater than the CG strike densities of the downscaled grids. The NDLE values for the uplands in western Malianwa exhibit this pattern, where more upward and/or downward lightning can be triggered by topographic highpoint attachment (Warner et al. 2013).

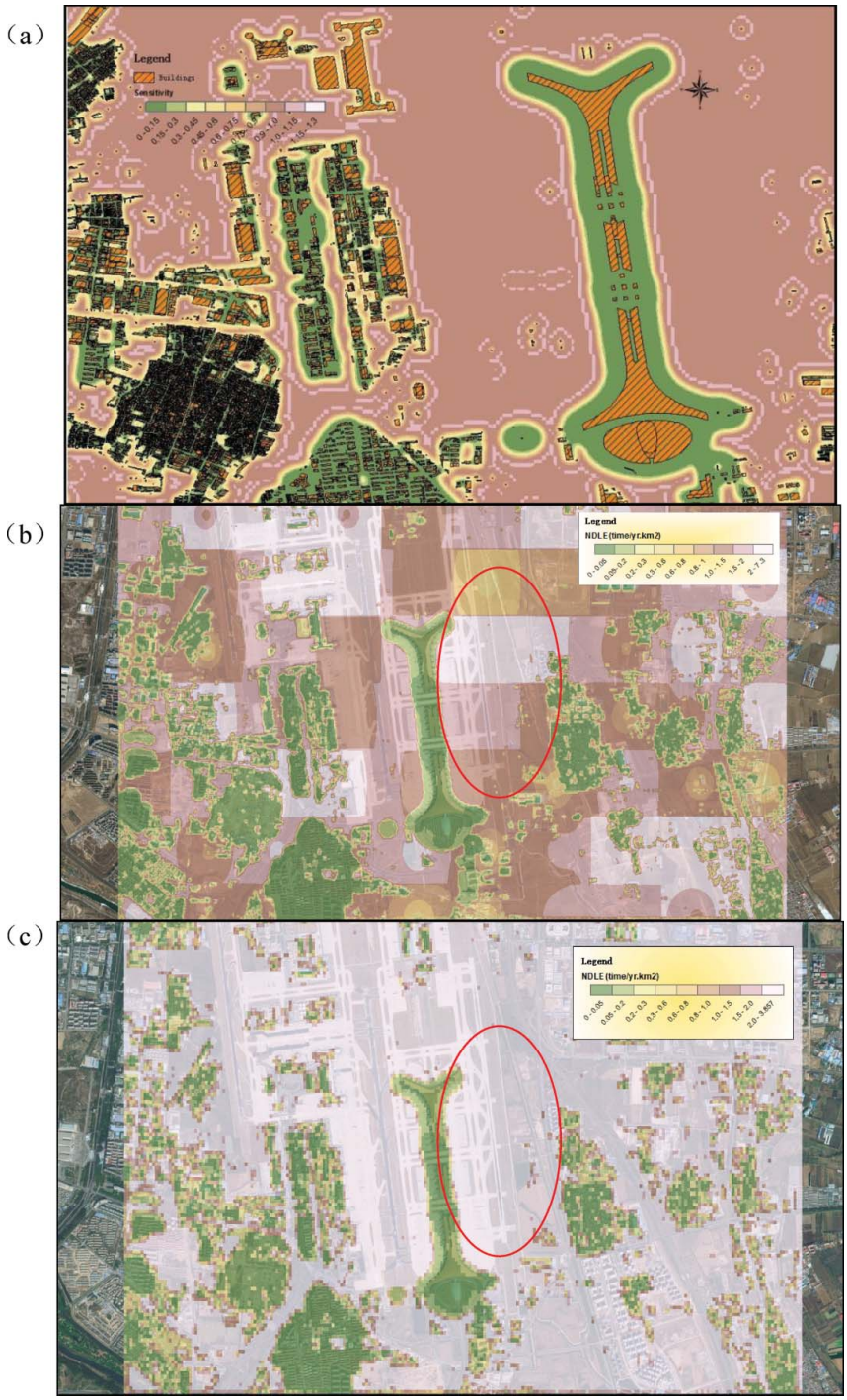

Figure 6. Lightning risk assessment of (a) ground sensitivity to lightning, (b) NDLE deduced using corrected CG strike density interpolated by IDW, and (c) NDLE deduced using corrected CG strike density estimated by kernel density method, for the Beijing International Airport. Obviously, the NDLE in (c) appears more smooth than that in (b), all displayed in Google Earth. (This figure is available in colour online.)

The advantage of quantitative risk assessment at high resolution is that its visualized risk characteristics can play an important role in operating risk control effectively. For instance, at the Beijing International Airport, terminal 3 (a 45 m high structure) and its nearby outdoor areas under structure canopies exhibit a low assessed sensitivity of 0.15, equivalent to 0.15 times that of an OFA, and NDLE values below 0.2 times/yr·km^2 (Figure 6). Conversely, the red ellipse in the aircraft parking apron, hundreds of metres away from the terminal, exhibits a high sensitivity of 1.0, and NDLE values above 1.0 time/yr·km^2 (in Figure 6(b)), or 2.0 time/yr·km^2 (in Figure 6(c)), due to the lack of lightning protection and structure shelter. On 11 August 2013, a lightning fatality occurred within the red ellipse (Figure 6(b)), when a cleaning staff member was struck dead by lightning while using a mobile phone (Hu 2014). Therefore, the personnel should pay attention to lightning on thunderstorm days when operating in open fields. Moreover, lightning risk management should be conducted based upon risk recognition in the airport community so that it can visually inform personnel regarding safe and unsafe areas (Figure 6).

6. Conclusion

The DE of a LLS cannot be 100%, and low DEs are usually due to a lack of deployed network sensors, as well as the performance and sensitivity of the sensors. Meanwhile, the signals produced by CG flashes can be strongly attenuated by long-distance propagation, terrain factors and underlying land surface conductivity. Before being used in NDLE estimates, the CG strike densities derived from LLS data should be corrected for DEs. Although the correction of CG strike density makes it better qualified for risk assessment, the LLS data should be made more reliable through network upgrades, which can improve the DE and location accuracy (Rudlosky and Fuelberg 2010). Moreover, network upgrades should be implemented not only for optimal lightning locating in metropolitan areas but also in mountainous rural areas, where more lightning casualties occur (López and Holle 1998; Curran et al. 2000; Zhang et al. 2011).

Uncertainty in lightning risk estimates at this high resolution is influenced by the LLS data quality related to locational precision and imperfect network DEs. Additionally, the model structures and operations (e.g. CG strike density downscaling) can magnify the uncertainty. Although the IDW interpolation and the overlapping of the derived CG strike density with the ground sensitivity to lightning may attenuate the errors in the risk estimate, uncertainty remains. However, it is suggested that the uncertainty caused by the LLS data quality can be reduced through network upgrades by adding high-performance and highly sensitive sensors. Further research can be undertaken to evaluate the reliability of the risk estimates in terms of the uncertainty (e.g. Monte Carlo simulation). Additionally, finding an effective approach for uncertainty reduction is also critical to identifying a more precise calibration and correction process in lightning risk assessment.

The model running at a fine resolution (e.g. a 5 m grid) can be used to accessibly assess lightning risk in terms of ground sensitivity for different types of underlying ground areas, and the data can be overlapped with CG strike density data. The lightning risk recognition at high resolutions can visually reveal risk discrepancies and indicate higher risk areas at a finer scale, making it favourable in lightning risk management.

This case study indicates that the lightning rod effects of structures produce outdoor areas of low risk under its canopy. In comparison, an OFA usually exhibits a higher risk, with an NLDE equal to the corresponding CG strike density and a sensitivity of nearly 1.0 in magnitude. The NLDE and sensitivity can differ by 1.15–1.3 times between uplands and the plains due to higher lightning attachment in elevated areas.

The distributions of lightning parameters (e.g. CG flash/strike density), ground sensitivity to lightning and NDLE comprehensively reveal lightning risk characteristics. The CG lightning flash/strike density, CG flash multiplicity, and other factors derived from LLS data not only indicate the regional lightning activity but also constitute the input parameters for lightning risk assessments. The sensitivity is correlated to the site-specific lightning protection capability the lightning

attractiveness of an earthen structure, and the lightning attachment induced by top terrains. This parameter indicates which parts of a residential sub-district are relatively prone to lightning strikes. The NDLE reflects lightning hazards, accounting for both regional lightning activity and sensitivity. The CG strike density, sensitivity and NLDE are practical indicators for decision-making in lightning risk management. They play important roles when taking effective actions to reduce site-specific lightning risks in residential sub-districts, e.g. erecting warning boards in high-risk areas, installing lightning protection facilities in the domains susceptible to lightning, and even constructing temporary structures serving as thunderstorm shelters in public OFAs.

Acknowledgements

We thank the two anonymous reviewers for their helpful comments on an earlier draft of this paper. Their good suggestion absolutely contribute to the improvement of our work.

Disclosure statement

No potential conflict of interest was reported by the authors.

Funding

This work has been supported by the Research Projects of Institute of Urban Meteorology, CMA [project number IUMKY201716]; Beijing Natural Science Foundation of China [grant number 8142019]; the Climate Change Research Projects of China Meteorological Administration [grant number CCSF201717].

References

Ashley WS, Gilson, CW. 2009. A reassessment of US lightning mortality. Bull Am Meteorol Soc. 90:1501–1518.

Bertram I, Mayr GJ. 2004. Lightning in the eastern Alps 1993–1999, part I: thunderstorm tracks. Nat Hazards Earth Syst Sci. 4:501–511. doi:10.5194/nhess-4-501-2004.

Biagi CJ, Cummins KL, Kehoe KE, Krider EP. 2007. National lightning detection network (NLDN) performance in southern Arizona, Texas, and Oklahoma in 2003–2004. J Geophys Res. 112:D05208. doi:10.1029/2006JD007341.

Bogdan A, Burcea C. 2010. A cloud-to-ground lightning climatology for Romania. Mon Weather Rev. 138:579–591. doi:10.1175/2009MWR2975.1.

Bourscheidt V, Pinto O Jr, Pinto IRCA, Naccarato KP. 2009. The influence of topography on the cloud-to-ground lightning density in South Brazil. Atmos Res. 91:508–513.

Bourscheidt V, Pinto O Jr, Naccarato KP. 2014. Improvements on lightning density estimation based on analysis of lightning location system performance parameters: Brazilian case. IEEE Trans Geosci Remote Sens. 52(3):1648–1657.

Changnon SA. 1985. Secular changes in thunder-day frequencies during the twentieth century. J Geophys Res. 90:6181–6194.

Changnon SA. 1993. Relationships between thunderstorms and cloud-to-ground lightning in the United States. J Appl Meteorol. 32:88–105.

Christian HJ, Blakeslee RJ, Boccippio DJ, Boeck WL, Buechler DE, Driscoll KT, Goodman SJ, Hall JM, Koshak WJ, Mach D, Stewart MF. 2003. Global frequency and distribution of lightning as observed from space by the optical transient detector. J Geophys Res. 108(D1):ACL 4-1-ACL 4-15. doi:10.1029/2002JD002347.

Cummins KL, Murphy JM, Bardo EA, Hiscox WL, Pyle BR, Pifer AE. 1998. A combined TOA/MDF technology upgrade of the U.S. National Lightning Detection Network. J Geophys Res. 103(D8):9035–9044.

Cummins KL, Cramer JA, Biagi CJ, Krider EP, Jerauld J, Uman MA, Rakov VA. 2006. The U.S. National Lightning Detection Network: post-upgrade status. Presented at: 2nd Conference on Meteorological Application of Lightning Data. Atlanta (GA): AMS Annual Meeting [cited 2013 Jan 31; 2006]. Available from: https://ams.confex.com/ams/pdfpapers/105142.pdf.

Cummins KL, Murphy JM. 2009. An overview of lightning locating systems: history, techniques, and data uses, with an in depth look at the US NLDN. IEEE Trans Electromagn Compat. 51:499–518.

Curran EB, Holle RL, Lopez RE. 2000. Lightning casualties and damages in the United States from 1959 to 1994. J Climate. 13:3448–3464.

Drüe C, Hauf T, Finke U, Keyn S, Kreyer O. 2007. Comparison of a SAFIR lightning detection network in northern Germany to the operational BLIDS network. J Geophys Res. 112:(D18114). doi:10.1029/2006JD007680.
Etherington TR, Perry GLW. 2017. Spatially adaptive probabilistic computation of a sub-kilometre resolution lightning climatology for New Zealand. Comput Geosci. 98:38–45.
Gabriel KR, Changnon SA. 1989. Temporal features in thunder days in the United States. Climatic Change. 15:455–477.
Hu H. 2014. An algorithm for converting weather radar data into GIS polygons and its application in severe weather warning systems. Int J Geogr Inf Sci. 28(9):1765–1780.
Hu H, Wang J, Pan J. 2014. The characteristics of lightning risk and zoning in Beijing simulated by a risk assessment model. Nat Hazards Earth Syst Sci. 14:1985–2014. doi:10.5194/nhess-14-1985-2014.
Hu H. 2015. Spatiotemporal characteristics of rainstorm-induced hazards modified by urbanization in Beijing. J Appl Meteorol Climatol. 54(7):1496–1509.
Holle RL, López RE, Navarro BC. 2005. Deaths, injuries, and damages from lightning in the United States in the 1890 s in comparison with the 1990 s. J Appl Meteorol. 44:1563–1573.
Idone VP, Davis DA, Moore PK, Wang Y, Henderson RW, Ries M, Jamason PF. 1998. Performance evaluation of the U.S. National Lightning Detection Network in Eastern New York; part I: detection efficiency. J Geophys Res. 103:9045–9056. doi:10.1029/98JD00154.
IEC62305-2. 2010. The technical committee of the International Electrotechnical Commission: protection against lightning. Geneva: IEC.
Kaplan S, Garrick BJ. 1981. On the quantitative definition of risk. Risk Anal. 1:11–27.
Kar SK, Liou YA. 2014. Enhancement of cloud-to-ground lightning activity over Taipei, Taiwan in relation to urbanization. Atmos Res. 147–148:111–120.
Krider EP, Noggle RC, Pifer AE, Vance DL. 1980. Lightning direction-finding systems for forest fire detection. Bull Am Meteorol Soc. 61(61):980–986.
López RE, Holle RL. 1998. Changes in the number of lightning deaths in the United States during the twentieth century. J Climate. 11:2070–2077.
Mäkelä A, Tuomi TJ, Haapalainen J. 2010. A decade of high−latitude lightning location: effects of the evolving location network in Finland. J Geophys Res. 115:(D21124). doi:10.1029/2009JD012183.
Mazarakis N, Kotroni V, Lagouvardos K, Argiriou AA. 2008. Storms and lightning activity in Greece during the warm periods of 2003–06. J Appl Meteorol. 47:3089–3098.
Mills B, Unrau D, Pentelow L, Spring K. 2010. Assessment of lightning-related damage and disruption in Canada. Nat Hazards. 52:481–499. doi:10.1007/s11069-009-9391-2.
Naccarato KP, Pinto O Jr. 2009. Improvements in the detection efficiency model for the Brazilian lightning detection network (BrasilDAT). Atmos Res. 91:546–563.
Petrov NI, D'Alessandro F. 2002. Assessment of protection system positioning and models using observations of lightning strikes to structures. Proc R Soc A. 458:723–742. doi:10.1098/rspa.2001.0906.
Rakov VA, Uman MA. 1990. Some properties of negative cloud-to-ground lightning flashes versus strike order. J Geophys Res. 95(D5):5447–5453.
Rizk FAM. 1994. Modelling of lightning incidence to tall structures, part II, application. IEEE Trans Power Delivery. 9:172–193.
Rose LS, Stallins JA, Bentley ML. 2008. Concurrent cloud-to-ground lightning and precipitation enhancement in the Atlanta, Georgia (United States), urban region. Earth Interact. 12:1–30. doi:10.1175/2008EI265.1.
Rudlosky S, Fuelberg HE. 2010. Pre- and postupgrade distributions of NLDN reported cloud-to-ground lightning characteristics in the contiguous United States. Mon Weather Rev. 138:3623–3633.
Saraiva ACV, Saba MMF, Pinto O Jr, Cummins KL, Krider EP, Campos LZS. 2010. A comparative study of negative cloud-to-ground lightning characteristics in São Paulo (Brazil) and Arizona (United States) based on high-speed video observations. J Geophys Res. 115:(D11102). doi:10.1029/2009JD012604.
Schulz W, Cummins KL, Diendorfer G, Dorninger M. 2005. Cloud-to-ground lightning in Austria: a 10-year study using data from a lightning location system. J Geophys Res. 110:D09101. doi:10.1029/2004JD005332.
Schütte T, Cooray V, Israelsson S. 1988. Recalculation of lightning location system acceptance using a refined damping model. J Atmos Oceanic Technol. 5:375–380.
Schütte T, Salka O, Israelsson S. 1987. The use of the Weibull distribution for thunderstorm parameters. J Climate Appl Meteorol. 26:457–463.
Shepherd JM, Pierce H, Negri AJ. 2002. Rainfall modification by major urban areas: observations from spaceborne rain radar on the TRMM satellite. J Appl Meteorol. 41:689–701.
Smith K. 1996. Environmental hazards: assessing risk and reducing disaster. 2nd ed. New York (NY): Routledge.
Stallins JA, Bentley ML, Rose LS. 2006. Cloud-to-ground flash patterns for Atlanta, Georgia (USA) from 1992 to 2003. Climate Res. 30:99–112.
Stallins JA, Rose LS. 2008. Urban lightning: current research, methods, and the geographical perspective. Geogr Compass. 2:620–639. doi:10.1111/j.1749-8198.2008.00110.x.

Steiger SM, Orville RE, Huffines G. 2002. Cloud-to-ground lightning characteristics over Houston, Texas: 1989–2000. J Geophys Res. 107(D11):ACL 2-1–ACL 2-9. doi:10.1029/2001JD001142.

Visacro S, Vale MHM, Correa G, Teixeira A. 2010. Early phase of lightning currents measured in a short tower associated with direct and nearby lightning strikes. J Geophys Res. 115:(D16104). doi:10.1029/2010JD014097.

Vogt BJ. 2011. Exploring cloud-to-ground lightning earth highpoint attachment geography by peak current. Earth Interact. 15:1–16.

Warner T, Helsdon JH Jr, Bunkers MJ, Saba MMF, Orville RE. 2013. Upward lightning triggering study. Bull Am Meteorol Soc. 94(5):631–635.

Zhang W, Meng Q, Ma M, Zhang Y. 2011. Lightning casualties and damages in China from 1997 to 2009. Nat Hazards. 57:465–476.

Yao W, Zhang Y, Meng Q, Wang F, Lu W. 2012. A Comparison of the characteristics of total and cloud-to-ground lightning activities in hailstorms. Acta Meteor Sinica. 27(2):282–293.